JOURNAL OF NANOMATERIALS AND DEVICES
Jul-Dec 2025, VOL. 3, ISSUE 2, pp. 27-32
https://doi.org/10.61577/jnd.2025.1000010

RESEAPRO JOURNALS

ORIGINAL ARTICLE

OPEN ACCESS

Photocatalytic degradation of chromium by $BiVO_4$-CoPc-nRGO nanocomposite

Shaikh Sohail

Department of Chemistry, Institute of Technical Education and Research, SOA University, Odisha, India

ABSTRACT

Background:
Photocatalytic degradation has emerged as a promising strategy for eliminating hazardous contaminants from aquatic environments. Chromium (VI) remains a critical pollutant of concern due to its high toxicity and carcinogenic properties, posing significant risks to human health and ecological systems. Advancements in visible-light-responsive photocatalysts offer new avenues for efficient remediation.

Objectives:
This study investigates the synthesis, characterization, and photocatalytic performance of a bismuth vanadate–cobalt phthalocyanine–nitrogen-doped reduced graphene oxide ($BiVO_4$–CoPc–nRGO) nanocomposite for the degradation of C (VI) in water.

Methods:
The nanocomposite was synthesized through a rapid and cost-effective hydrothermal approach. Structural and morphological assessments were conducted using X-ray diffraction (XRD), scanning electron microscopy (SEM), and complementary analytical techniques to confirm phase composition and surface architecture. Photocatalytic activity was evaluated under visible light irradiation, and reduction efficiency toward Cr (VI) was quantified. Recyclability and operational stability were examined through multiple photocatalytic cycles.

Results:
Characterization confirmed the successful formation of a distinct $BiVO_4$–CoPc–nRGO composite with well-defined structural features conducive to enhanced charge separation and visible-light activity. The material demonstrated high photocatalytic efficiency in reducing Cr (VI), attributable to synergistic interactions among the composite components. Stability tests indicated minimal performance loss across repeated cycles, affirming its robustness and reusability.

Conclusion:
The $BiVO_4$–CoPc–nRGO nanocomposite exhibited strong photocatalytic activity, durability, and operational stability under visible light, underscoring its potential for practical deployment in chromium-contaminated water treatment. The findings provide a foundation for further development of composite photocatalysts for sustainable environmental remediation.

KEY WORDS

Nanocomposite; Chromium; Degradation; Irradiation; Cobalt; Bismuth; Contamination

ARTICLE HISTORY

Received 13 November 2025;
Revised 04 December 2025;
Accepted 10 December 2025

Introduction

The considerable industrial expansion is contributing to an increase in the contamination of dangerous metals. Because of chromium's significant contribution to chemical emissions and toxicity to microorganisms, plants, and animals, it is of ecological significance. Numerous sectors, including the dyeing and printing of textiles, chemical production, leather tanneries, metal plating, and the processing of industrial effluents that harmed live cells, release significant amounts of chromiuminto the surrounding environment [1]. There are two different types of chromium ions: Cr (VI) and Cr (III). In contrast to Cr (VI), which is highly poisonous and carcinogenic, mutagenic, and teratogenic to both humans and animals, Cr (III) is less harmful and readily deposited as Cr (OH)3. Cr (VI)is only allowedin wastewater at a maximum level of 0.05 mg L-1. The development of efficient wastewater treatment techniques is crucial to eradicating refractory organic pollutants and reducing Cr (VI) to Cr (III) [2] The efficiency, cost, and secondary pollution produced by conventional chromium removal treatment techniques such chemical precipitation, ion exchange, and adsorption are all severelyrestricted. Therefore, it is crucialto find effective and long-lasting methods forremoving chromium. By converting Cr (VI) to Cr (III) and degrading organic pollutants, heterogeneous photocatalysis offers a potentialoption for detoxifying organiccontaminants and Cr (VI) from wastewater [2] Due to its excellent performance, moderate reaction conditions, and ecologically friendly nature, photocatalytic degradation has become a viable method for the remediation of many contaminants, including heavy metals. To neutralize the target contaminants, photocatalysis uses a photocatalyst that can absorb light energy and produce electron-hole pairs. These electron-hole pairs subsequently take part in redox reactions. Precipitation, ion exchange, photocatalysis, reverseosmosis, and an adsorption processare all components of the chromium removal technique. Most ofthese techniques demandsubstantial upfront and ongoing costs, making them unsuitable for small companies. In comparison to the other techniques listed, photocatalysis is the most efficient and affordable. One possible method for either oxidizing or reducing dangerous contaminants is photocatalysis [1].

*Correspondence: Mr. Shaikh Sohail, Department of Chemistry, Institute of Technical Education and Research, SOA University, Odisha, India,
email: sohailshaikh8093@gmail.com

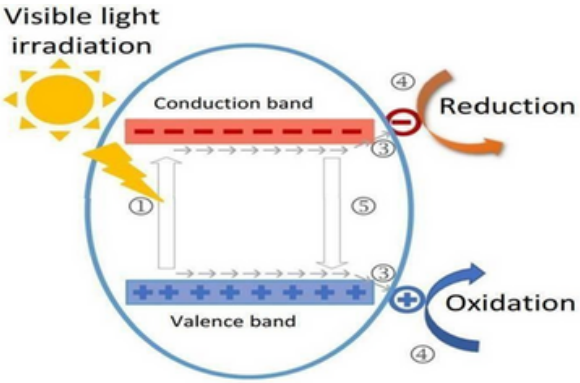

Figure 1. Simplified mechanism for the photocatalysisofsemiconductor catalysts.

Bismuth vanadate ($BiVO_4$) has attracted a lot of attention among the diverse group of semiconductor photocatalysts as visible-light-driven photocatalyst. $BiVO_4$ has good bandgap energy (2.4 eV) that makes it possible to absorb visible light and utilize solar radiation effectively. Additionally, $BiVO_4$ has strong photocatalytic activity, limited toxicity, and great chemical stability. $BiVO_4$ broad bandgap, however, reduces the photocatalytic productivity of the material since it can only absorb a tiny portion of the solar spectrum. $BiVO_4$ has been used in a variety of ways to improve photocatalytic activity, including the addition of sensitizers, co-catalysts, and conductive supports. One method that shows promise combines metal-organic compounds like phthalocyanines synergistically with $BiVO_4$ [3]. Numerous studies have been conducted on cobalt phthalocyanine (CoPc), a metal-organic complex with significant visible light absorption, good stability, and effective transfer capabilities. In addition to CoPc, carbon-based materials have attracted a lot of attention when used as co- catalysts or supports in photocatalysis. Reduced graphene oxide (RGO), one of graphene's derivatives, has gained recognition for its high stability, huge specific surface area, and outstanding electron transport capabilities. Due to its higher photocatalytic activity and charge separation efficiency, nitrogen-doped reduced graphene oxide (nRGO) has received special interest [4]. In the current study, we suggest using a new nanocomposite made of BiVO4, CoPc, and nRGO to photocatalyze the chromium's decomposition. By combining $BiVO_4$, inoPc, and nRGO into a single nanocomposite, researchers hope to make use of their complementary properties and overcome the drawbacks of the separate components. The main photocatalyst, BiVO4, oversees generating charges and absorbing light. When CoPc is used as a co- catalyst, photogenerated pairs of electrons and holes may be separated more effectively, accelerating redox processes. The conductive base nRGO, on the other hand, boosts electron transport and offers a large surface area for the adsorption of chromium compounds.

Materials and Methods

In the present study, bismuth vanadate ($BiVO_4$), cobalt phthalocyanine (CoPc), and reduced graphene oxide (rGO) were synthesized as precursor materials for the preparation of the final composite photocatalyst. $BiVO_4$ was synthesized via the hydrothermal method, wherein bismuth and vanadium precursors were reacted in an aqueous medium under elevated temperature and pressure, leading to the nucleation and crystallization of $BiVO_4$ [5]. CoPc was prepared using the solvothermal technique, employing pyromellitic dianhydride, urea, and DBU (1,8-diazabicyclo[5.4.0]undec-7-ene) in a three-neck flask under high-pressure and high-temperature conditions to facilitate condensation and cyclization for the formation of the cobalt phthalocyanine structure. For the synthesis of rGO, 0.2 g of graphene oxide was dispersed in 100 mL of deionized water and ultrasonicated until a clear, uniform solution was obtained. Subsequently, 0.25 mL of hydrazine hydrate and 0.36 g of urea were added, and the reaction mixture was maintained at 100°C for 8 hours in an oil bath under reflux with continuous N_2 sparging [6]. The resulting black solid was filtered using a G3 funnel, washed thoroughly with deionized water and methanol, and dried at 65°C for 24 hours to obtain the reduced graphene oxide. These synthesized materials were further utilized for the preparation of the target composite material.

The $BiVO_4$–CoPc–NrGO nanocomposite was synthesized through a hydrothermal process involving sequential preparation and combination of precursor solutions. Initially, the precursor solutions were prepared by dissolving 1.97 g of bismuth nitrate pentahydrate ($Bi(NO_3)_3{\cdot}5H_2O$) in a mixture of ethanol and 50 mL of deionized (DI) water to obtain the Bi precursor, while 0.786 g of vanadium chloride (VCl_3) was dissolved in 50 mL of DI water to form the V precursor solution [7]. Separately, 0.3 g of cobalt phthalocyanine (CoPc) was dissolved in ethanol to obtain the CoPc precursor solution, and 0.5 g of nitrogen-doped reduced graphene oxide (NrGO) was dispersed in DI water by ultrasonication to achieve a homogeneous NrGO suspension. These prepared precursor solutions were then combined in a suitable container and stirred magnetically for a defined duration to ensure uniform mixing and interaction among all components [8].

The resulting homogeneous mixture was transferred into a Teflon-lined stainless-steel autoclave, which was sealed tightly to prevent leakage. The autoclave was then placed in an oven and maintained at the desired temperature and pressure for a specific duration to facilitate the hydrothermal reaction. Upon completion of the reaction, the autoclave was allowed to cool naturally to room temperature, followed by careful depressurization in accordance with standard safety procedures. The obtained product was collected by decanting the mixture into centrifuge tubes and centrifuging at an appropriate speed to separate the solid nanocomposite from the supernatant [9]. The precipitated $BiVO_4$–CoPc–NrGO nanocomposite was repeatedly washed with DI water to remove residual impurities, with centrifugation performed after each washing step. Finally, the purified nanocomposite was dried either in air or in an oven at a controlled temperature until a constant weight was achieved, yielding the final composite material [10].

Analysis method

A chromium stock solution was prepared by dissolving 141.4 mg of potassium dichromate ($K_2Cr_2O_7$) in 100 mL of distilled water to obtain a 500-ppm solution. A 100-ppm solution was then prepared by dilution, followed by 25, 50, 75, and 100 ppm standard solutions prepared by further diluting to 25 mL each. Figure 2 shows stock and standard solutions [11].

The diphenyl carbazide (DPC) reagent was prepared by dissolving 25 mg of DPC in 5 mL of acetone and storing it in a brown bottle. In an acidic medium, DPC reacts with Cr^{6+} to produce a pink-colored complex, whose intensity indicates chromium concentration [Figure 3] [12].

https://doi.org/10.61577/jnd.2025.1000010

About 5 mL of orthophosphoric acid was taken in a 10 mL beaker to acidify the chromium solution, enabling proper DPC reaction and color formation. A 1 N NaOH solution was prepared by dissolving 2 g of NaOH pellets in 50 mL of deionized water for pH adjustment during analysis [13].

Figure 2. Chromium stock solution and five standard solutions.

Figure 3. Colour of reduced Chromium solution at time variation.

Results and Discussions

The results section presents the quantitative analysis of chromium reduction efficiency at a concentration of 25ppm and a reaction time of 120 minutes. The reduction efficiency is calculated by comparing the initial chromium concentration with the residual chromium concentration after the reaction [Table 1 and Figure 4].

Table 1: Standard concentrations (mg/L) of chromium with corresponding absorbance values at 540 nm.

Std(mg/L)	Abs(540nm)
0.2	0.171
0.3	0.262
0.4	0.403
0.5	0.363
0.6	0.531
0.7	0.512
0.8	0.535

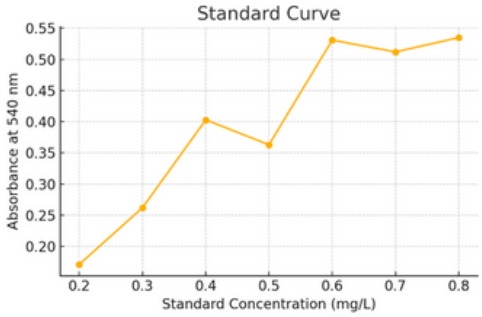

Figure 4. Standard curve between concentration and absorbance at 540 nm.

This result concluded that at 120 min of reaction with the nanocomposite under direct sunlight it yielded the maximum degradation for the 25mg/L sample concentration [Table 2] [14].

Table 2. Chromium degradation data at 90 and 120 minutes.

Conc (mg/L)	Abs (540nm)	Degradation %	Conc (mg/L)	Abs (540nm)	Degradation %
90 Mins			120 Mins		
Control	0.51	36.4	Control	0.578	25
25	0.88	0	25	0.37	61.5
50	0.451	46.2	50	0.543	31
75	0.5	38.5	75	0.682	6.65

Then pH variation was done by taking a constant conc of 25mg/L at acidic and neutral pH of 2, 4, 6 and 7, because in basic medium there will no H+ ions for carrying out any reduction reactions [Table 3] [15].

Table 3. Chromium degradation at different pH levels at different periods.

pH	Dark	30min	60min	90min	120min
Control	a- 0.958 % d- 0	a- 0.526 % d- 27.2	a- 0.504 % d- 30.56	a- 0.551 % d- 23.37	a- 0.772 % d- 0
2	a- 0.894 % d- 0	a- 0.292 % d- 62.84	a- 0.321 % d- 58.44	a- 0.268 % d- 66.49	a- 0.262 % d- 67.5
4	a- 0.861 % d- 0	a- 0.401 % d- 46.24	a- 0.386 % d- 48.52	a- 0.441 % d- 40.13	a- 0.349 % d- 54.16
6	a- 0.805 % d- 0	a- 0.352 % d- 53.72	a- 0.392 % d- 47.60	a- 0.402 % d- 46.08	a- 0.813 % d- 0
7	a- 0.617 % d- 13.32	a- 0.361 % d- 52.36	a- 0.417 % d- 43.79	a- 0.464 % d- 36.64	a- 0.590 % d- 17.43

Kinetics of chromium reduction

The Langmuir–Hinshelwood kineticmodel can be simplified to an apparentfirst-order kinetics model as follows:

$$\ln\frac{C_o}{C_t} = K_r K_t = K_{app} t$$

where Kapp stands for the apparent first-order rate constant (min^{-1}) of chromium reduction. From equation (3) the apparentrate constant, Kapp can be calculated from the slope of the plot between ln (C_0/C_t) versus time [16].

Thid equation depicts the relationship between 1/Kapp and the starting concentration of chromium (C_0). It is noted that the experimental data fits the Langmuir-Hinshelwood kinetic model well with a higher R2 (0.99) value for the correlation coefficient [17].

$$\frac{1}{K_{app}} = \frac{1}{KK_r} + \frac{C_o}{K_r}$$

As reducing agent concentration decreases, the kineticsof chromium reduction decreases.

Chromium reduction reactions can beaccelerated by catalysts, resultingin higher rates of reaction. Moreover, other substances in the reactionmixture, such as organic compounds or complexing agents, may affect the kinetics of chromium reduction by stimulating or inhibiting it [18].

Reduction reactioncan also occur inan ordered fashiondepending on the specific conditions and mechanisms involved.

Reduction kinetic at different initial concentrations of chromium

The graph clearlydepicts that in the dark conditions, there is an insignificant decrease in the concentration of chromium,

https://doi.org/10.61577/jnd.2025.1000010

but under visible light irradiation chromium reduction percentage reached the highest value at 67.5 % [Figure 5] [14,18,19].

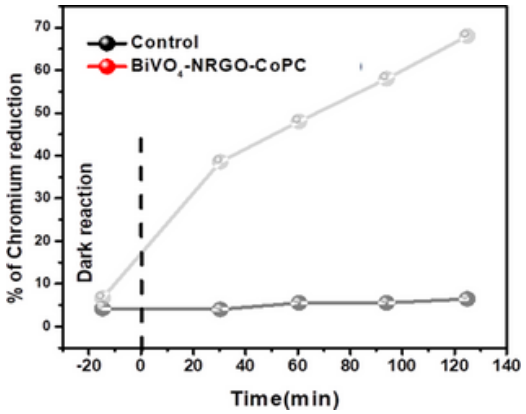

Figure 5. Standard graph showing the chromium concentration % in dark and light conditions.

Demonstration of chromiumreduction profiles

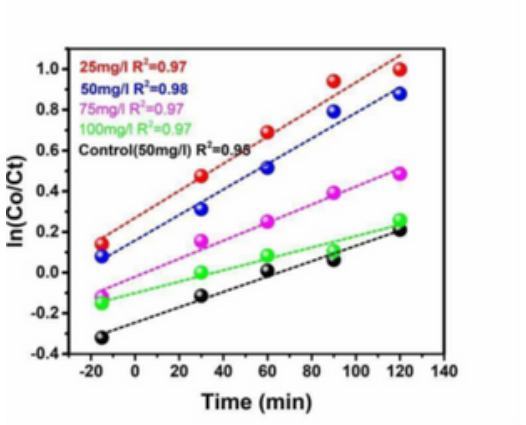

Figure 6. Kinetic plot for photocatalytic degradation of Cr^{6+}.

Figure 6shows that as the initial concentration of chromium decreases its $\ln(C_o/C_t)$ linear slope goes on increasing.

Pseudo first order kinetic of chromium

As the valueof highest reduction was shown for 25 mg/L of chromiumsolution, hence its 1/Kapp value will be at the bottom of the graph [Figure 7] [20].

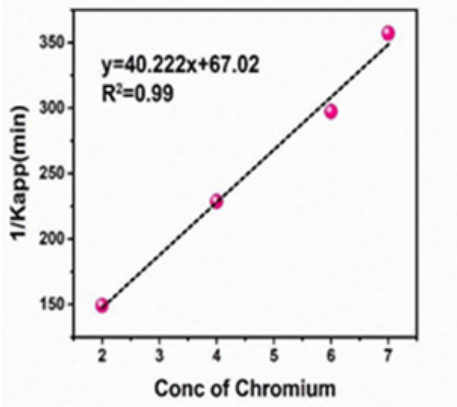

Figure 7.Linear relationship between chromium concentration and $1/k_a$pp.

Characterization data

XRD characterization of $BiVO_4$

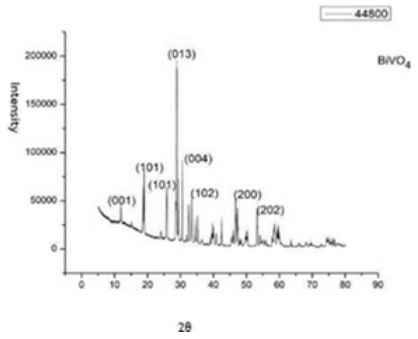

Figure 8.X-ray diffraction of $BiVO_4$.

- X-ray diffraction (XRD) characterization of BiVO4 provides valuable insights into its crystal structure. The XRD pattern displays distinctive peaks at 2θ values of 11.95 °,18.97, 25.8° , 28.7, 30.5° , 46.67° ,53.24 °and 58.55°were indexed to (001), (101), (101), (013), (004) and (200), (202), (212) planes respectively [Figure 8].
- Shows Distorted tetragonal structure.
- Peaks are matched to JCPDS card #00-006-0249 and 01-083-1699.

XRD characterization of CoPc

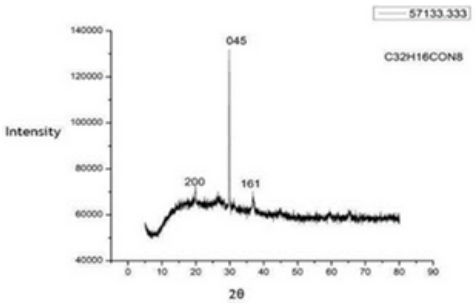

Figure 9.X-ray diffraction of CoPc.

- X-ray diffraction (XRD) characterization of BiVO4 provides valuable insights into its crystal structure. The XRD pattern displays distinctive peaks at 2θ values of 12.9°, 29.86°, 36.80°, were indexed to (200), (045), (161) planes respectively [Figure 9].
- Shows orthorhombic structure.
- Peaks are matched to JCPDS card 96-412-8818 and 96-810-3638.

XRD characterization of GO

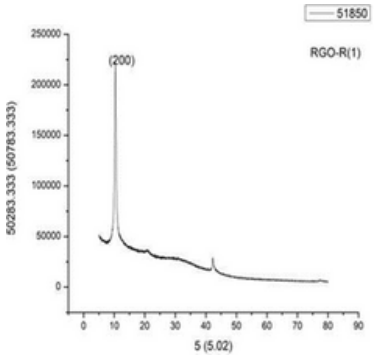

Figure 10.X-ray diffraction of GO.

https://doi.org/10.61577/jnd.2025.1000010

GO peak of GO at around 10.8°, suggest that the graphite oxidized successfully, especially that peaks at 24.5° originating from removal of oxygen atoms inserting into graphite gallery [Figure 10].

XRD characterization of NrGO

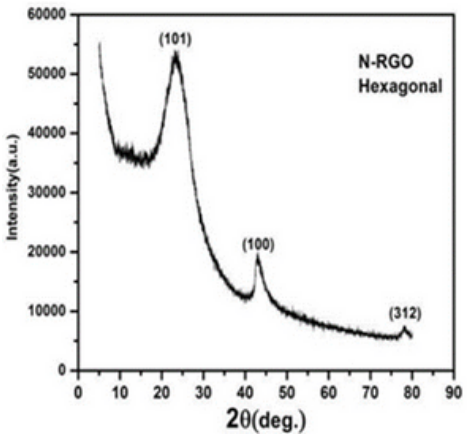

Figure 11.X-ray diffraction of NrGO.

- N-rGO peaks at 43° (100) due to the change of the structure for graphene sheet. The order of relative intensity of 100 peak is NrGO>rGO>GO [Figure 11].
- The peak is associated with sp3 bonding.
- The border peak is the larger interlayer distance. N-rGO further increases the interlayer distance, bettering more specific areas and active sites.

FE-SEM OF $BIVO_4$

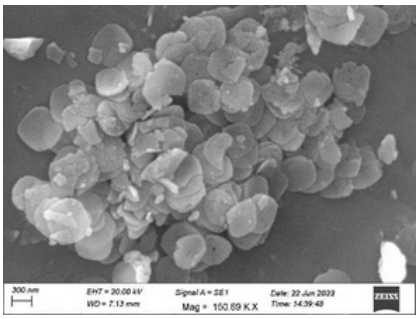

Figure 12.FE-SEM image of $BiVO_4$.

FE-SEMimaging of $BiVO_4$ exposes the topography and texture of the surfaceof the substance. It demonstrate the presence of distinctive characteristics as uniform plateau-like structure that corresponds to uniform surface area for pollutant adsorption [Figure 12] [21].

FE-SEM OF CoPc

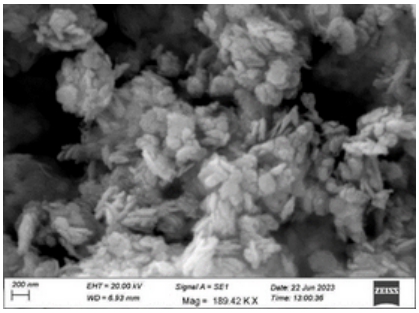

Figure 13.FE-SEM image of CoPc.

FE-SEMimaging of CoPc exposes the topography and texture of the surface of the substance. It demonstrate the presence of distinctive characteristics as uniform rod-like structure that corresponds to better support and overall photosensitization phenomena [Figure 13] [22].

FE-SEM OF NrGO

In addition to itsporous 3D structure, N-rGO had an exfoliated and corrugated surface. Due to the stacking characteristic of graphene, this corrugated structure is thought to result from the reduction of graphene to rGO and the removal of oxygen-containing groups from the surface. This material is exfoliated and subsequently intercalated with epoxy, carboxyl, and hydroxyl functional groups. It has a highly wrinkled structure. The average size of GO was estimated at 500-700 nm [Figure 14] [23].

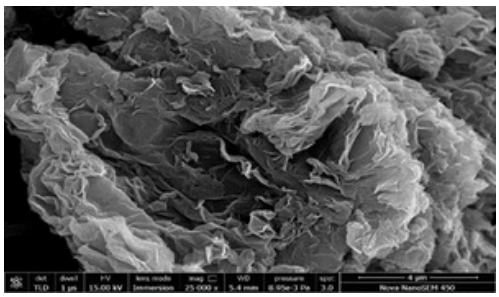

Figure 14.FE-SEM image of NrGO.

FE-SEM OF $BIVO_4$-CoPc-NrGO nanocomposite

The cracks and crevices are all occupied by the NrGO and the small disc shaped structures on the surface are nothing but the $BiVO_4$ and all the rod-like structures that are below the disc shaped particles are all CoPc photosensitizer [Figure 15] [24].

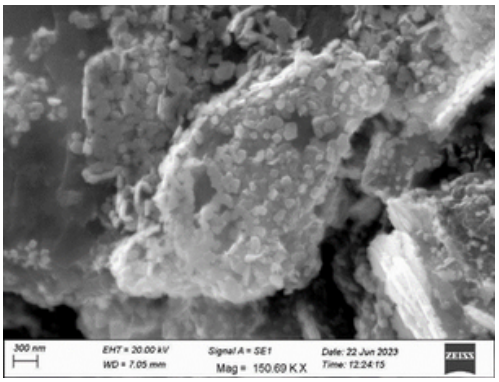

Figure 15.FE-SEM image of $BIVO_4$-CoPc-NrGO nanocomposite.

Conclusions

By using $BiVO_4$-CoPc-NrGO nanocomposite the maximum degradation of chromium of conc. 25 mg/L that we got was67.5 % at pH 2 from120 minutes of start of reaction under visible light. Sunlight is green energy and infinite energy resource. Using sunlight by the photocatalyst $BiVO_4$ modified with CoPc and NrGO the heavy metal Chromium was removed. The photocatalyst was prepared by hydrothermal and solvothermal methods. By introduction of CoPc, its visible light harvestation efficiency increased. Hence its photocatalytic activity increased.The metal is characterized by X-ray Diffraction (XRD). Different concentrations of the Chromium solution were analyzed. It is shown that the 25mg/L of the

https://doi.org/10.61577/jnd.2025.1000010

chromium shows maximum reduction. Different parameters such as catalyst amount, pH of the solution, time of light irradiation. At pH2 under 2 hours of sunlight irradiation the maximumreduction occurs, that is 67.5%.

Disclosure Statement

No potential conflict of interest was reported by the author.

References

1. Kangralkar MV, Manjanna J, Momin N, Rane KS, Nayaka GP, Kangralkar VA. Photocatalytic degradation of hexavalent chromium and different staining dyes by ZnO in aqueous medium under UV light. Environ Nanotechnol Monit Manage. 2021;16:100508. https://doi.org/10.1016/j.enmm.2021.100508
2. Zhang Q, Wang M, Ao M, Luo Y, Zhang A, Zhao L, et al. Solvothermal synthesis of Z-scheme AgIn5S8/Bi2WO6 nano-heterojunction with excellent performance for photocatalytic degradation and Cr (VI) reduction. J. Alloys Compd. 2019;805:41-49. https://doi.org/10.1016/j.jallcom.2019.06.331
3. Liu Y, Duan S, Liu J, Jin X, Dong F, Shi G, et al. One-dimensional shaving-like BiVO4 nanobelts: Synthesis, characterization and photocatalytic activity with methylene blue. Molecules. 2023;28(23):7793. https://doi.org/10.3390/molecules28237793
4. Soltani T, Tayyebi A, Lee BK. Efficient promotion of charge separation with reduced graphene oxide (rGO) in BiVO4/rGO photoanode for greatly enhanced photoelectrochemical water splitting. Sol Energy Mater Sol Cells. 2018;185:325-332. https://doi.org/10.1016/j.solmat.2018.05.050
5. Monfort O, Badurova K, Motola M, Roch T, Satrapinskyy L. Investigation of the photocatalytic properties of bismuth vanadate-based materials for promising environmental remediation. Student Scientific Conference PriF UK 2017. Proceedings of reviewed contributions. 2017:1025-1030.
6. Zhang JX, Hu CY, Wang W, Wang H, Bian ZY. Visible light driven reduction of CO2 catalyzed by an abundant manganese catalyst with zinc porphyrin photosensitizer. Appl Catal A Gen. 2016;522:145-151. https://doi.org/10.1016/j.apcata.2016.04.035
7. Kaur R, Sharma S, Kaur H. Heavy metals toxicity and the environment. J Pharmacogn Phytochem. 2019;1:247-249.
8. Araucz K, Aurich A, Kołodyńska D. Novel multifunctional ion exchangers for metal ions removal in the presence of citric acid. Chemosphere. 2020;251:126331. https://doi.org/10.1016/j.chemosphere.2020.126331
9. Stoller M, Sacco O, Vilardi G, Pulido JO, Di Palma L. Technical–economic evaluation of chromium recovery from tannery wastewater streams by means of membrane processes. Desalin Water Treat. 2018;127:57-63. https://doi.org/10.5004/dwt.2018.22533
10. Staszak K, Kruszelnicka I, Ginter-Kramarczyk D, Góra W, Baraniak M, Lota G, Regel-Rosocka M. Advances in the removal of Cr (III) from spent industrial effluents—A review. Materials. 2022;16(1):378. https://doi.org/10.3390/ma16010378
11. Bayuo J. An extensive review on chromium (vi) removal using natural and agricultural wastes materials as alternative biosorbents. J Environ Health Sci Eng. 2021;19(1):1193-1207. https://doi.org/10.1007/s40201-021-00641-w
12. Aziz NA, Palaniandy P, Aziz HA, Dahlan I. Review of the mechanism and operational factors influencing the degradation process of contaminants in heterogenous photocatalysis. J Chem Res. 2016;40(11):704-712. https://doi.org/10.3184/174751916X14769685673665
13. Srivastava R, Sofi IR. Impact of synthetic dyes on human health and environment. Impact of textile dyes on public health and the environment. 2020:146-161. https://doi.org/10.4018/978-1-7998-0311-9.ch007
14. Borges ME, Sierra M, Méndez-Ramos J, Acosta-Mora P, Ruiz-Morales JC, Esparza P. Solar degradation of contaminants in water: TiO2 solar photocatalysis assisted by up-conversion luminescent materials. Sol Energy Mater Sol Cells. 20161;155:194-201. https://doi.org/10.1016/j.solmat.2016.06.010
15. Sang Y, Liu H, Umar A. Photocatalysis from UV/Vis to near-infrared light: towards full solar-light spectrum activity. ChemCatChem. 2015;7(4):559-573. https://doi.org/10.1002/cctc.201402812 Advanced https://doi.org/10.1016/B978-0-12-810499-6.00006-1
16. Deng Y, Feng C, Tang L, Zeng G, Chen Z, Zhang M. Nanohybrid photocatalysts for heavy metal pollutant control. Nanohybrid and Nanoporous Materials for Aquatic Pollution Control. 2019:125-153. https://doi.org/10.1016/B978-0-12-814154-0.00005-0
17. Khan MM, Pradhan D, Sohn Y, editors. Nanocomposites for visible light-induced photocatalysis. Cham, Switzerland: Springer International Publishing; 2017. https://doi.org/10.1007/978-3-319-62446-4
18. Hunge YM, Yadav AA. Basics and advanced developments in photocatalysis—A review (Mini review). Int. J. Hydrol. 2018;2(4):539-540.
19. Mandade P. Introduction, basic principles, mechanism, and challenges of photocatalysis. Handbook of nanomaterials for wastewater treatment. 2021:137-154. https://doi.org/10.1016/B978-0-12-821496-1.00016-7
20. Jonas F, Lebeau B, Michelin L, Carteret C, Josien L, Vidal L, et al. Thermal stability and phase transformation of semi-crystalline mesostructured TiO2 in the presence of heteroelements. Micropor Mesopor Mat. 2021;315:110896. https://doi.org/10.1016/j.micromeso.2021.110896
21. Karuppanan KK, Panthalingal MK, Biji P. Nanoscale, catalyst support materials for proton-exchange membrane fuel cells. Handbook of nanomaterials for industrial applications. 2018:468-495. https://doi.org/10.1016/B978-0-12-813351-4.00027-4
22. Deb M, Sarkar SC. Issues of Sustainable Development in the Mines and Minerals Sector in India. Minerals and Allied Natural Resources and Their Sustainable Development: Principles, Perspectives with Emphasis on the Indian Scenario. 2017:519-551.
23. Meng X, Eluagwule B, Wang M, Wang L, Zhang J. Solar photocatalysis for environmental remediation. Handbook of smart photocatalytic materials 2020:183-195. https://doi.org/10.1016/B978-0-12-819049-4.00013-1
24. Manchala S, Elayappan V, Lee HG, Shanker V. Plasmonic photocatalysis: An extraordinary way to harvest visible light. InPhotocatalytic Systems by Design 2021 (pp. 187-216). Elsevier. https://doi.org/10.1016/B978-0-12-820532-7.00015-1

https://doi.org/10.61577/jnd.2025.1000010